Available online at www.sciencedirect.com
ScienceDirect
Journal of the European Ceramic Society 27 (2007) 2245–2253
www.elsevier.com/locate/jeurceramsoc

Self-propagating high-temperature synthesis of barium titanate and subsequent densification by spark plasma sintering (SPS)

Roberta Licheri [a], Sarah Fadda [a], Roberto Orrù [a,b,*], Giacomo Cao [a,b,**], V. Buscaglia [c]

[a] *Dipartimento di Ingegneria Chimica e Materiali, Centro Studi sulle Reazioni Autopropaganti (CESRA), Unità di Ricerca del Consorzio Internazionale Nazionale per la Scienza e Tecnologia dei Materiali (INSTM), Università degli Studi di Cagliari, Piazza D'Armi 09123, Cagliari, Italy*

[b] *PROMEA Scarl, c/o Dipartimento di Fisica, Cittadella Universitaria di Monserrato, S.S. 554 bivio per Sestu, 09042 Monserrato, CA, Italy*

[c] *Istituto per l'Energetica e le Interfasi, Consiglio Nazionale delle Ricerche, via De Marini 6, I-16149 Genova, Italy*

Received 18 May 2006; received in revised form 1 August 2006; accepted 10 August 2006
Available online 26 September 2006

Abstract

This paper describes the self-propagating high-temperature synthesis (SHS) of perovskitic oxides, specifically $BaTiO_3$, and their subsequent densification by spark plasma sintering. With the final goal of obtaining dense nanostructured materials, SHS products were mechanically treated at different milling time conditions, before densification. It was found that the grain size of ball milled powders decreases with increasing milling time, this effect being more evident at early stages of milling. Depending upon the ball milling (BM) conditions adopted, crystallite size in the range 15–70 nm was obtained. After milling for 5 h, the resulting powders (20–30 nm) were sintered by SPS, at 700 A, for different periods of time. By properly varying sintering time in the interval 70–140 s, it is possible to obtain products with relative density in the range 66–99%, respectively. In particular, grain growth during sintering was found to be limited (below 50 nm) if the electric current is applied for time intervals equal to or less than 100 s. The observed dielectric properties are typical of a nanocrystalline $BaTiO_3$ ceramic.

Keywords: SHS; SPS sintering; Grain size; Dielectric properties; $BaTiO_3$ and titanates

1. Introduction

It is well known that barium titanate ($BaTiO_3$) and $BaTiO_3$-based ceramics have attracted considerable attention especially for their dielectric properties.[1–7] Above the Curie temperature (125 °C) the structure of barium titanate is that of a cubic perovskite. Below this temperature, the structure is slightly distorted and three ferroelectric polymorphs (tetragonal, orthorhombic and rhombohedral) with non-zero dipole moment exist depending on temperature.[8] The hexagonal phase does not have a perovskite structure and is only stable at temperatures >1429 °C.

It is also well established that the properties of this kind of material strongly depend on structure and grain size.[7,9–14] These materials are typically obtained in powder form by several methods, including hydrothermal synthesis, aqueous combustion, sol–gel techniques or precipitation from aqueous solution.[10,11,15] Thus, in order to obtain dense products, a consolidation step is subsequently required. Regarding consolidation processes, it is known that high density $BaTiO_3$ products with fine grain size (<100 nm) are difficult to obtain because of grain growth taking place during the final stage of densification processes.[11]

Although all synthesis methods mentioned above can yield high purity fine powders characterized by low degree of agglomeration and narrow size distribution, several steps which require long processing times are typically involved.[16,17]

* Corresponding author at: Dipartimento di Ingegneria Chimica e Materiali, Università degli Studi di Cagliari, Piazza D'Armi 09123, Cagliari, Italy. Tel.: +39 070 6755076; fax: +39 070 6755057.
** Corresponding author at: Dipartimento di Ingegneria Chimica e Materiali, Università degli Studi di Cagliari, Piazza D'Armi 09123, Cagliari, Italy. Tel.: +39 070 6755058; fax: +39 070 6755057.
E-mail addresses: orru@visnu.dicm.unica.it (R. Orrù), cao@visnu.dicm.unica.it (G. Cao).

0955-2219/$ – see front matter © 2006 Elsevier Ltd. All rights reserved.
doi:10.1016/j.jeurceramsoc.2006.08.004

In this study, barium titanate has been synthesized by self-propagating high-temperature synthesis (SHS). This technique is based on the occurrence of highly exothermic reactions which, once ignited by means of external energy sources for relatively short times, propagate in the form of a combustion wave leading to final products progressively without requiring additional energy.[18,19] SHS represents an attractive method for materials synthesis due to the simplicity of the process and its low energy requirements, the high purity of products, as well as the possibility of obtaining complex or metastable phases. A wide variety of advanced materials, such as ceramics, intermetallics, composites, solid solutions, etc., have been successfully obtained in very short processing times (order of seconds).

Thus, since the reaction for barium titanate formation starting from BaO_2, Ti and TiO_2 is sufficiently exothermic to guarantee the self-propagation of the combustion front,[20] the SHS method represents, in principle, an efficient route to synthesize such material.

In order to obtain nanostructured powders, a mechanical treatment by ball milling (BM) of SHS products is also performed before the densification step. Mechanical treatment by BM involves cold-welding, fracturing phenomena and comminution of processed powders and was demonstrated to be an extremely versatile technique allowing for the production of nanostructured products for advanced materials science and technology.[21]

Dense $BaTiO_3$ products with fine grain size were recently obtained by spark plasma sintering (SPS) starting from powders prepared by the different chemical methods mentioned above.[11–14,22–25] This is a relatively novel sintering technique based on the simultaneous application of a pulsed dc current and uniaxial mechanical load through powdered samples.[26,27] Another recent approach consists of combining mechanosynthesis of $BaTiO_3$ nanopowders with SPS.[28]

It is worth noting that SPS typically enables a compact to be sintered under more uniform heating conditions, lower temperature and relatively shorter sintering periods, as compared with conventional methods.[29,31] In particular, the latter two aspects allow grain growth to be minimized.[26,29–33] Along these lines, in this work barium titanate powders obtained by SHS and mechanically treated to reach the desired nanostructure, are then densified by SPS apparatus. The influence of SPS time on densification, crystallite size and transition phase evolution is systematically investigated in this paper. In addition, the obtained products are characterized in terms of dielectric properties.

2. Experimental materials and methods

The characteristics and sources of reactants used for the synthesis of perovskite oxide powders are reported in Table 1.

The starting mixtures to be processed by SHS were prepared by mixing reactants according to the following reaction:

$$BaO_2 + 0.5Ti + 0.5TiO_2 = BaTiO_3 \quad (1)$$

Starting powders were mixed in acetone, used as dispersing agent, for 2 h. About 10 g of the resulting mixture were uniaxially pressed to form cylindrical pellets (16 mm diameter and 20 mm height), with green density of about 50% of the theoretical value (6.02 g/cm^3).

Table 1
Properties of reactants used for $BaTiO_3$ synthesis

Reactant	Source	Particle size	Purity (%)
BaO_2	Aldrich	−325 mesh	95
TiO_2 (anatase)	Aldrich	−325 mesh	–
Ti	AEE	20 μm	99.7

The experimental set-up used in this work for SHS is described in detail elsewhere.[34] Briefly, the combustion front was generated at one sample end by using of a heated tungsten coil, which was immediately turned off as soon as the reaction was initiated. Then, the reaction self-propagates until reaches the opposite end of the pellet. The temperature during reaction evolution was measured using thermocouples (W-Re, 127 mm diameter, Omega Engineering Inc.). About 5 g of the obtained SHS products were milled (SPEX mixer mill 8000) with two steel balls (13 mm diameter, 8 g weight) for different milling time intervals (30 min, 5, 15 h). It should be noted that the iron content in milled powders was evaluated by means of ICP-OES (VISTA MPX-VARIAN) and resulted to be less than 0.25 wt.%.

Ball milled powders were then sintered in the form of disks by Spark Plasma Sintering Machine (SPS 515 Sumitomo Coal Mining Co. Ltd.), whose schematic representation is reported in Fig. 1. Typically, 5 g of milled SHS powders to be consolidated were poured into a cylindrical graphite die (15 mm inside diameter, 30 mm outside diameter, 30 mm height, AT101 graphite, ATAL s.r.l., Italy). Between the sample and the internal surface of the die, a graphite foil (0.13 mm thick, purity 99.8%, Alfa Aesar) was placed in order to facilitate sample extraction after SPS process. In addition, with the aim of minimizing heat losses by thermal radiation, the die was covered with a layer of graphite felt. The die was then placed inside the reaction chamber of the SPS apparatus and the system was evacuated (10 Pa). This step was followed by the application of a mechanical pressure through the plungers.

The SPS apparatus combines a 50 kN uniaxial press with a dc pulsed generator (10 V, 1500 A, 300 Hz) to simultaneously provide a pulsed electric current through the sample and the graphite die containing it, together with a mechanical load through the die plungers (diameter 14.7 mm, 20 mm height, AT101 graphite, ATAL s.r.l., Italy). Two cylindrical graphite blocks (diameter 80 and 30 mm, and height 40 and 20 mm, respectively, AT101 graphite, ATAL s.r.l., Italy) were placed between the upper plunger and upper electrode.

During the entire SPS process, a mechanical pressure of 40 MPa was maintained through the plungers, and an electrical current of 700 A was applied for different periods of time. Thus, the obtained products have been characterized in terms of density in order to follow the sintering evolution. Temperature was measured during sintering by a C-type thermocouple, which was inserted inside a small hole in one side of the graphite die. Temperature, applied current, voltage, mechanical load and the

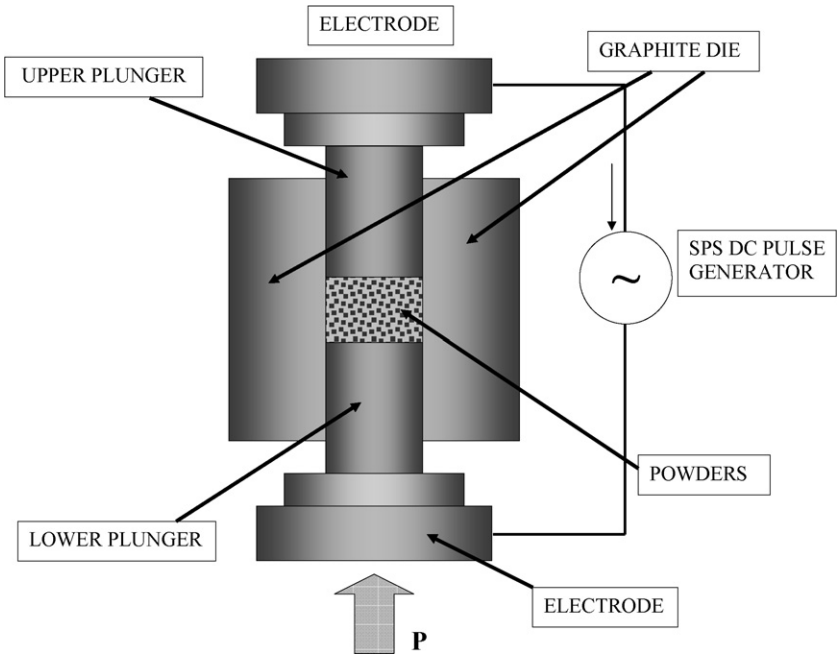

Fig. 1. Schematic representation of spark plasma sintering (SPS) system.

vertical displacement of the lower electrode were measured in real time and recorded.

Density of sintered samples was determined by the Archimedes' method, while grain size was calculated from XRD data by means of the Halder and Wagner method.[35] The latter makes it possible to separate the two contributions to diffraction line broadening, namely, the refinement of crystallite size and the internal strain, as follows:

$$\left(\frac{B^*(f)}{d^*}\right)^2 = \frac{B^*(f)}{d^{*2}}\frac{1}{L} + \left(\frac{\eta}{2}\right)^2 \quad (2)$$

where $B^*(f) = B(f)\cos(\theta)/\lambda$, $d^* = 2\sin(\theta)/\lambda$, $B(f)$ is the half-maximum breadth of the diffraction profile, θ the Bragg angle, λ the X-ray wavelength, L the crystallite size and η is the strain factor. Thus, by plotting $(B^*(f)/d^*)^2$ versus $B^*(f)/d^{*2}$, a straight line is obtained. The slope of this line gives the inverse of the average crystallite size, L, and its intercept provides the value of the internal strain.

Powder and dense product characterization was performed in terms of chemical composition and microstructure by X-ray diffraction (XRD) analysis (Philips 1830 diffractometer using Cu Kα Ni-filtered radiation), scanning electron microscopy (SEM) and electron dispersive spectroscopy (EDS) analysis (Hitachi S4000 Field Emission equipped with Kevex Sigma 32 Probe, resolution of 142 eV). Specifically, the identification of diffraction phases was performed using PCPDFWIN Version 2.0 according to search routines on the basis of data index powders diffraction file.[36]

Before dielectric measurements, thin slices (thickness: ≈0.1 cm) with parallel surfaces were cut from the sintered samples, polished and then annealed in air for 24 h at 800 °C. This treatment was intended to relieve the residual stresses (arising either from SPS process or from polishing) and remove the surface carbon contamination. The graphite die used for densification can induce reducing sintering conditions with oxygen loss from the lattice and an increase in conductivity. Therefore, a further objective of the post-annealing treatment is to remove the excess of oxygen vacancies and improve dielectric properties. Dielectric measurement was performed by means of an impedance analyzer (Solatron SI1260) with an applied voltage of 1 V, in the frequencies range 0.1–100 kHz, by varying temperature between 40 and 170 °C (heating/cooling rate 0.5 °C/min). Sputtered gold electrodes were applied on the upper and lower surfaces of the sample, thus obtaining a parallel plate capacitor configuration.

3. Results and discussion

3.1. Synthesis and ball milling of $BaTiO_3$

According to its high enthalpy of reaction (1), i.e. $-\Delta H_r^\circ = 556.142$ kJ/mol,[37] synthesis of $BaTiO_3$ displayed a self-propagating behaviour. A typical temperature profile recorded during combustion synthesis by a thermocouple embedded in the sample is reported in Fig. 2. It is apparent that the temperature suddenly increases when the wave approaches to the position where the thermocouples are placed, thus reaching its maximum value, equal to about 1800 °C.

Since the melting point of $BaTiO_3$ is 1616 °C,[37] a liquid phase is formed. Consistently, it was found that the reacting pellet changes its shape during combustion synthesis occurrence. After the maximum temperature is reached, it decreases, with a relatively smaller rate, although rather rapidly, until reaching room temperature. Front velocity was calculated from temperature profiles and was approximately equal to 20 mm/s.

The diffraction patterns of reactants, and SHS products, either unmilled or ball milled at different time periods, are reported in

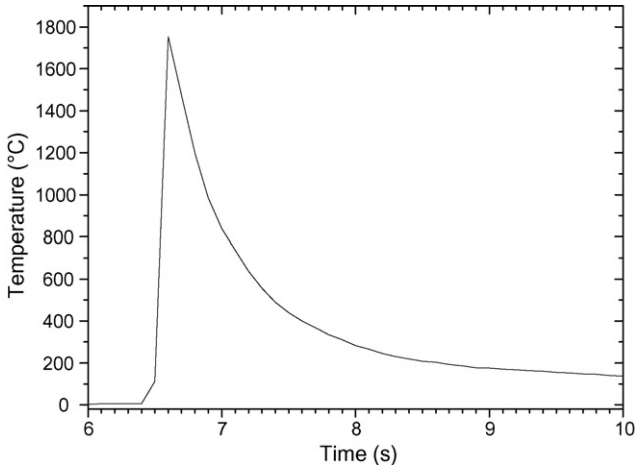

Fig. 2. Temperature profile recorded during SHS of $BaTiO_3$.

Fig. 3. Phase analysis of diffraction patterns showed that reaction proceeds to completion with the formation of hexagonal $BaTiO_3$.

The obtained product is black/blue coloured as an indication, albeit indirect, of the formation of oxygen deficient hexagonal $BaTiO_3$.[38,39] This is justified by the experimental conditions, i.e. high-temperature, rapid cooling, inert environment, under which the product is prepared.

It should be also noted that, among the possible different $BaTiO_3$ phase modifications, the hexagonal one is stable only when $T \geq 1429\,^{\circ}C$.[40] Therefore, the product formed during this reaction is metastable at room temperature, as a consequence of the rapid cooling and the reducing conditions.[39,41] As shown in Fig. 3, after ball milling, diffraction patterns were characterized by well shaped peaks, with peak broadening an indication of the refinement of the structure. From the analysis of the line broadening and the full width at the half maximum of XRD signals in a large range of 2θ, grain size and strain are reported in Fig. 4. The figure shows the crystallite size refinement and

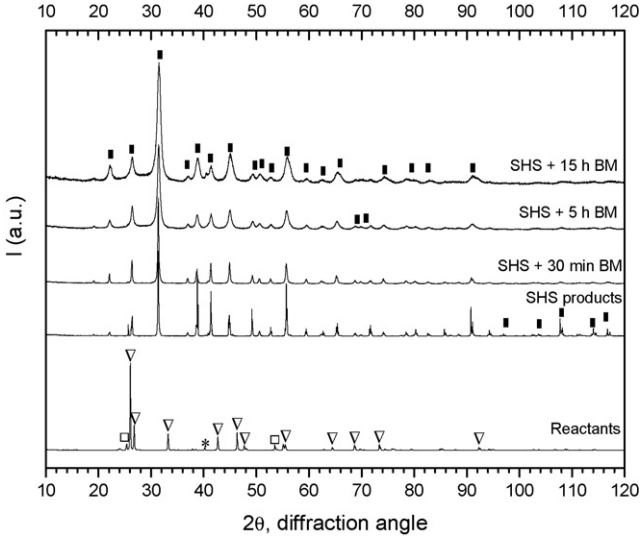

Fig. 3. XRD patterns of starting reactants and SHS products either unmilled or ball milled at different time periods: (■) $BaTiO_3$ (82–1175), (▽) BaO_2, (□) TiO_2, (*) Ti.

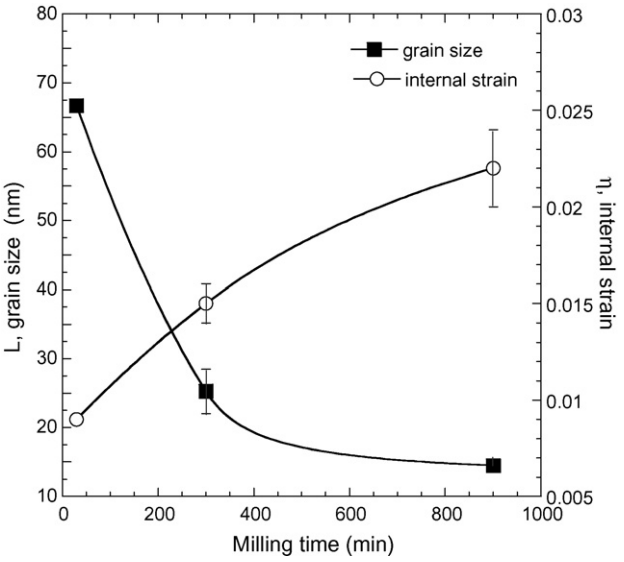

Fig. 4. Effect of milling time on crystallite size and strain of $BaTiO_3$ powders obtained by SHS.

the strain increase as functions of milling time. After 30 min of milling, the average grain size was equal to about 66 nm and reached 15 nm at 15 h. Slightly smaller (9 nm as determined by Scherrer formula) $BaTiO_3$ crystallite size has been obtained by mechanochemical treatment starting from the same reactants as used in this work after 72 h in a planetary mill.[28]

SHS milled powders have been also characterized by SEM. As an example, secondary electron SEM images of the 5 and 15 h ball milled powders are reported in Fig. 5a and b, respectively. It is shown that after milling, $BaTiO_3$ consists of soft agglomerated particles with sizes in the range of 1–10 μm.

On the basis of the obtained results, it seems that both grain and particle sizes change more significantly within 5 h milling. Therefore, powders milled for such a time period have been subsequently used for sintering purposes.

3.2. Densification of $BaTiO_3$ powders

SPS experiments performed using powders ball milled for 5 h were conducted in vacuum, at 700 A, under a mechanical pressure of 40 MPa. Samples investigated in the present work were sintered by SPS at different time intervals in the range of 0–140 s. Fig. 6 shows the SPS outputs, i.e. current, voltage, temperature and sample displacement, as a function of sintering time, when the application of the electric current was interrupted after 140 s. After reaching its maximum value, voltage decreasing (cf. Fig. 6a) can be related to the increase of the system temperature (cf. Fig. 6b) encountered during this stage, which is accompanied by a decrease of its electrical resistivity. Although the slope of temperature–time curve seems to decrease as SPS time was increased, thermal equilibrium is not reach within the temporal range, i.e. 0–140 s, considered in this study.

The displacement profiles shown in Fig. 6b, reveal that during the first 30 s, i.e. before the current reaches 700 A, the system did not show any noteworthy shrinkage. The maximum sample

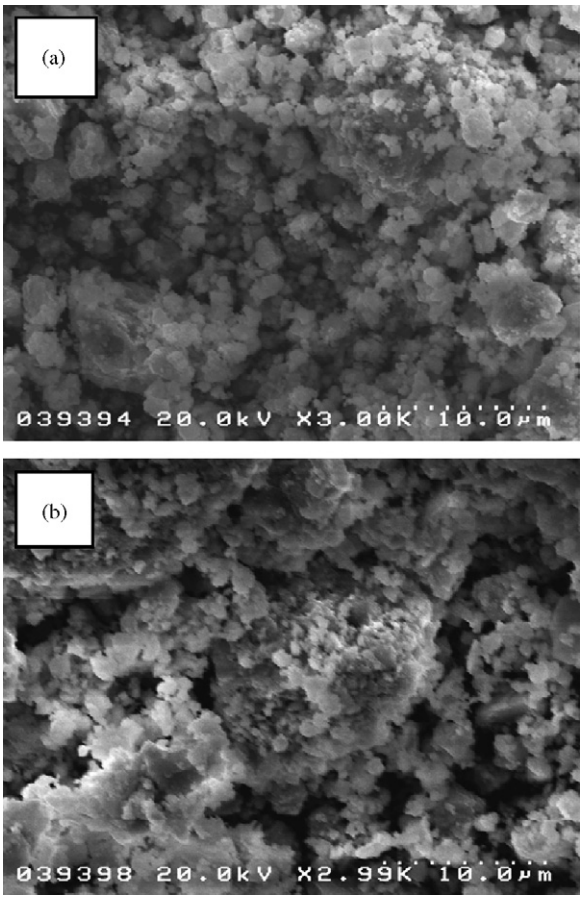

Fig. 5. SEM secondary electrons micrographs of ball milled powders, corresponding to (a) milling time = 5 h, and (b) milling time = 15 h.

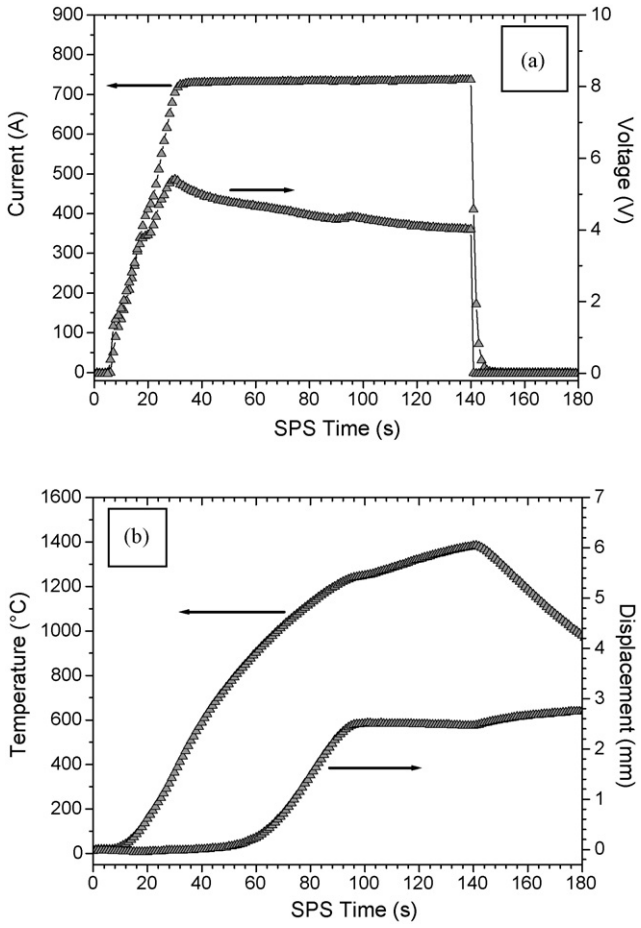

Fig. 6. Temporal profiles of SPS outputs: (a) current intensity and voltage and (b) temperature and sample displacement (I = 700 A, P = 40 MPa, t = 140 s).

displacement is attained when the temperature is in the range 1200–1300 °C (Fig. 6b). As shown in Fig. 7, where the effect of SPS time on relative density is reported, the ceramic products with relative density in the range of about 65–98% can be obtained by varying the sintering time from 70 to 140 s, respectively.

This aspect is strictly related to the corresponding maximum temperature level reached during the process, also shown in Fig. 7 as a function of the sintering time. Polished and fracture surfaces of SPS samples were investigated by SEM and the results corresponding to 70 and 140 s are reported in Fig. 8a and b, respectively. It is seen that while a near full dense material was obtained at 140 s, the sample resulting after 70 s still did not have the aspect of a bulk product. Moreover, the observation of fracture surfaces reveals that a significant crystallite growth accompanies the sintering process in the 70–140 s SPS time interval.

XRD patterns of SPS products obtained at different processing time periods are reported in Fig. 9. It is seen that as SPS time is increased, the corresponding XRD profiles display relatively narrower peaks when compared to starting powders. The results achieved by applying the Halder and Wagner method to the XRD patterns of SPS products, obtained when the electric current was applied for time periods in the range 0–100 s, are shown in Fig. 10.

The SPS treatment affects in a relatively modest manner the $BaTiO_3$ grain sizes which are maintained below 50 nm.

Beside the variation of crystallite size and strain, another aspect to be considered is the possible modification of $BaTiO_3$ configuration during sintering. It was stated that the product formed after SHS, and maintained during the BM treatment, was hexagonal $BaTiO_3$. The latter one is a metastable phase,

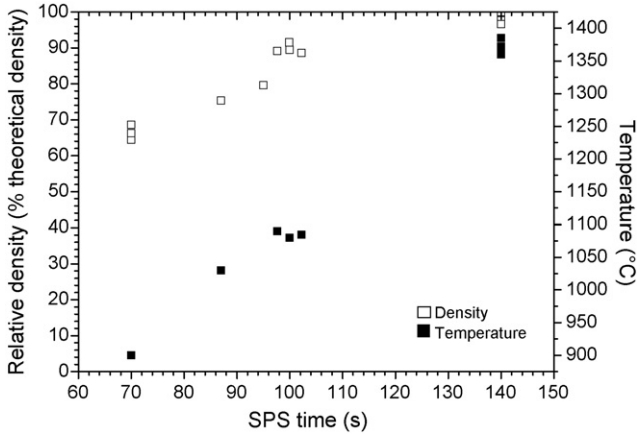

Fig. 7. Effect of SPS time on relative density of sintered $BaTiO_3$ and the corresponding maximum temperature reached during the sintering process.

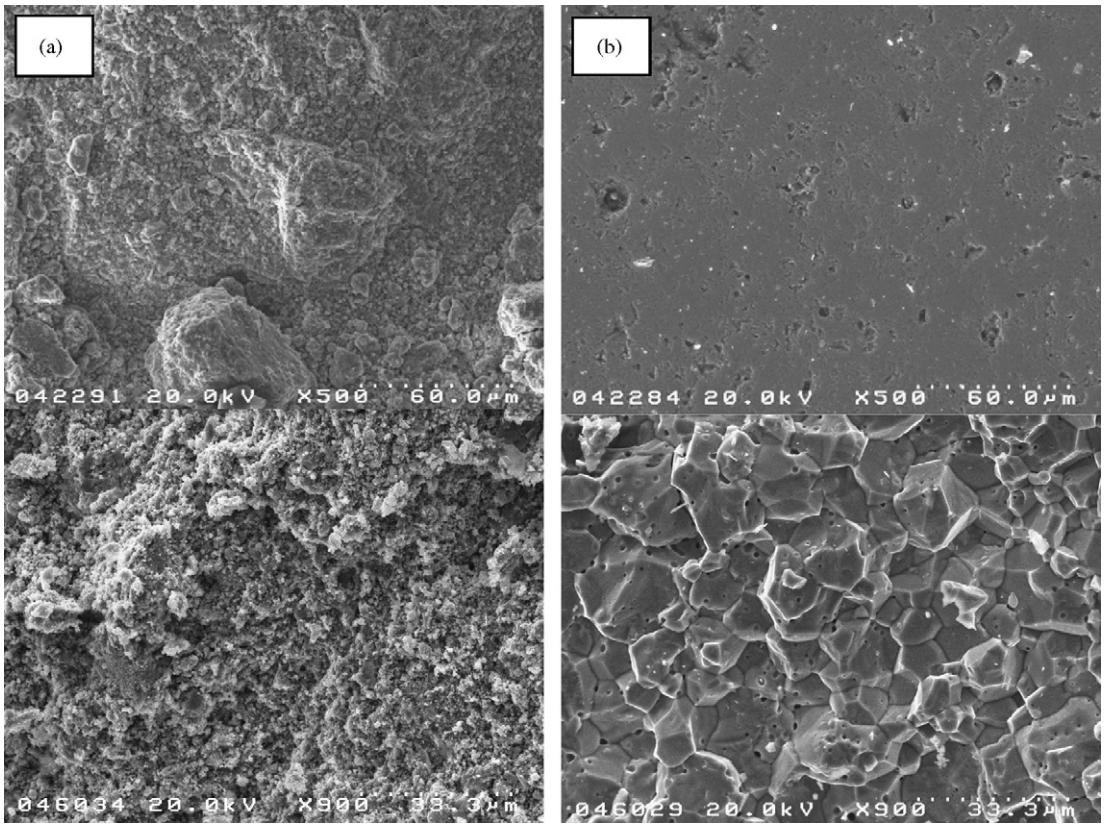

Fig. 8. Polished and fracture surfaces SEM secondary electrons micrographs images of two SPS end-products corresponding to (a) $t = 70$ s, and (b) $t = 140$ s ($I = 700$ A, $P = 40$ MPa).

thus it is likely it is transformed to the most stable one, i.e. the tetragonal, when the product is subjected to thermal treatment. Accordingly, as shown in Fig. 11 where a detailed view ($2\theta = 44$–47°) of XRD patterns of SPS products are reported as a function of sintering time, evidence of such transition is observed. Specifically, in this figure, typical peaks splitting characteristic of the tetragonal $BaTiO_3$ phase[11] is clearly seen, particularly when SPS time is prolonged to 140 s. Nevertheless, diffraction peaks of the hexagonal phase (cf. Fig. 9) appear to be already strongly reduced when the thermal treatment duration is 70 s.

It should be noted that, according to the phase diagram, the modification hexagonal → tetragonal should involve also the cubic phase, as intermediate configurations. However since the

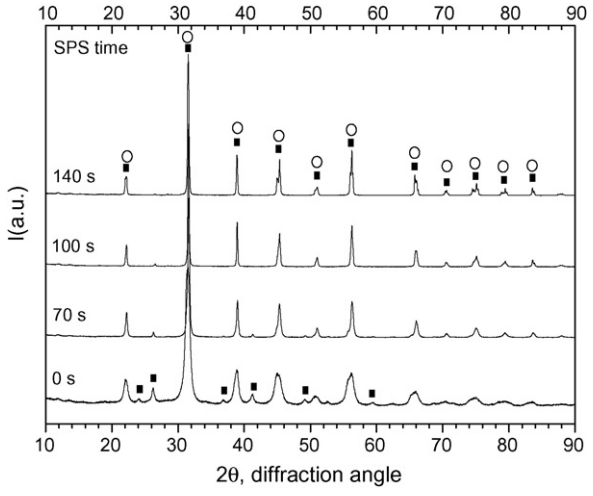

Fig. 9. XRD patterns of SPS products obtained at different values of the time interval during which the pulsed electric current was applied ($I = 700$ A, $P = 40$ MPa): (■) hexagonal $BaTiO_3$ (82–1175), (◯) tetragonal $BaTiO_3$ (81–2205).

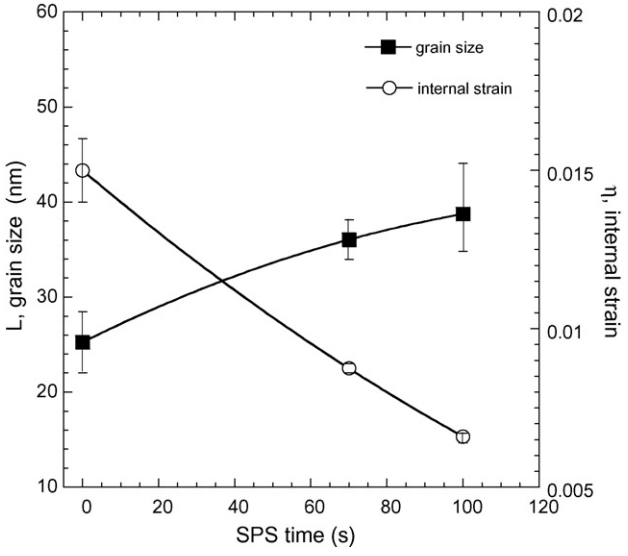

Fig. 10. Crystallite size and strain of $BaTiO_3$ products obtained by SPS as function of the sintering time.

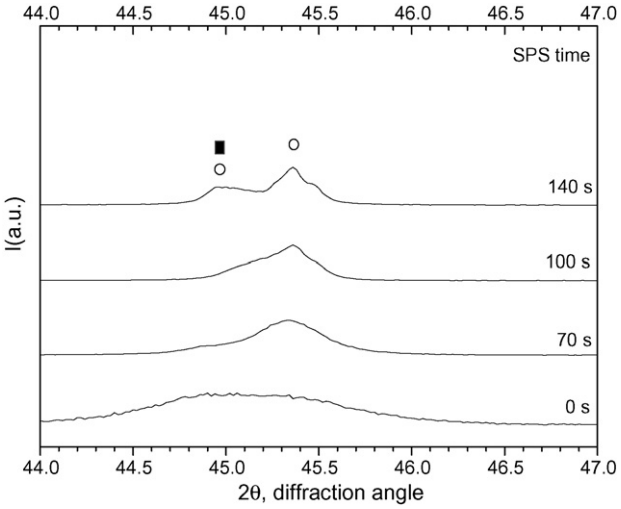

Fig. 11. Detail of XRD patterns of SPS products ($I = 700$ A, $P = 40$ MPa) in the 44–47° 2θ range, as a function of the holding time. The typical splitting of tetragonal $BaTiO_3$ is shown: (■) hexagonal phase (82–1175), (◯) tetragonal phase (81–2205).

majority of the diffraction lines of cubic $BaTiO_3$ are very close to those of the tetragonal phase, there is not a direct indication of its formation.

Regarding crystallite size analysis, the application of the Halder and Wagner method for SPS products obtained under such conditions (140 s), is made difficult because peaks are too narrow, the latter suggesting a significant increasing of crystallite size. This fact is consistent with the SEM findings discussed previously (Fig. 8b).

Accordingly, the observed phenomenon of peaks splitting mentioned above represents a well known, albeit indirect, indication of the increasing growth of $BaTiO_3$ crystallites.[11] Therefore, this time interval (140 s) may be considered as that one when grain growth starts to become significant.

3.3. Dielectric properties

The dielectric permittivity or relative dielectric constant, ε', and the dielectric loss tangent, $\tan\delta$, of the nanocrystalline ceramic sintered for 100 s, post-annealed in air and with a grain size of about 40 nm are shown in Figs. 12 and 13, respectively. In agreement with the general behavior reported in the literature,[9,13] the decrease of grain size leads to the broadening and flattening of the permittivity anomaly located at the ferroelectric-to-paraelectric transition temperature (T_C, Curie temperature). Consequently, the sharp peak of ε' located at T_C and typical of coarse ceramics[9] is replaced by a rounded maximum (Fig. 12), suggesting a more diffuse character of the phase transition. The position of the permittivity maximum, 108 °C, is significantly lower than the value of T_C, 125 °C, reported for single crystals and coarse ceramics,[8] and this is a consequence of the reduced grain size of the present material, in agreement with previous observations.[13] The loss tangent (Fig. 13) is relatively low, <5%, up to 110 °C. At higher temperatures there is a progressive increase in $\tan\delta$ for frequencies below 10 kHz. The

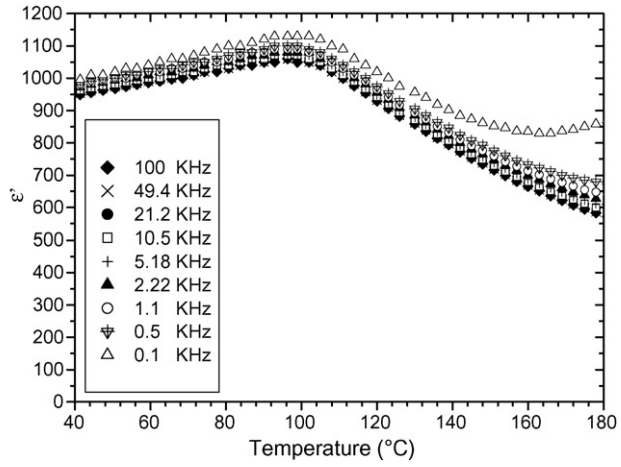

Fig. 12. Dielectric constant ε' as a function of temperature at frequencies in the range 0.1–100 kHz.

high losses, the strong frequency dispersion and the anomalous behaviour of ε' observed at 0.1 kHz indicate the existence of a space charge layer effect. This space charge layer is probably localized at the grain boundaries and originates from the partial inhomogeneity of the dielectric properties of the grains. Whilst the surface layer of the grains in contact with the grain boundaries is fully oxidized and insulating, the core of the grains is slightly oxygen deficient and more conductive. In the paraelectric region ($T > T_C$), for temperatures above 120 °C and frequencies ≥5 kHz (cf. Fig. 14), the permittivity is well described by the Curie–Weiss law:

$$\varepsilon' = \frac{C}{T - T_0} \tag{3}$$

where C is the Curie constant and T_0 is the Curie–Weiss temperature.

At lower frequencies there is a progressive departure from the Curie–Weiss law related to the space charge effect. The relative dielectric constant is significantly depressed in comparison to coarse ceramics. The peak value of ε' is around 1100, to be compared with values of the order of 5000–6000 reported for

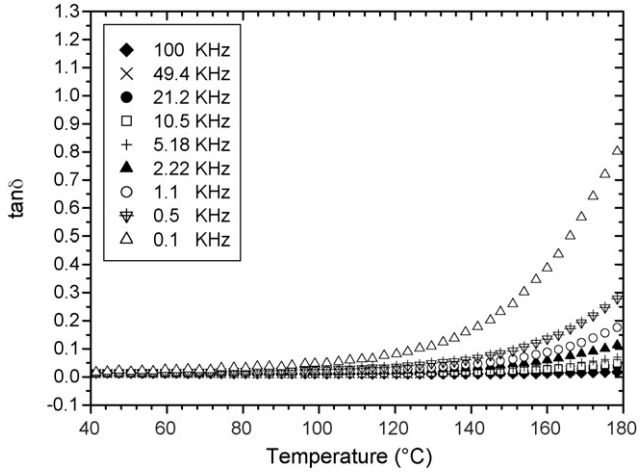

Fig. 13. Dielectric losses as a function of temperature at frequencies in the range 0.1–100 kHz.

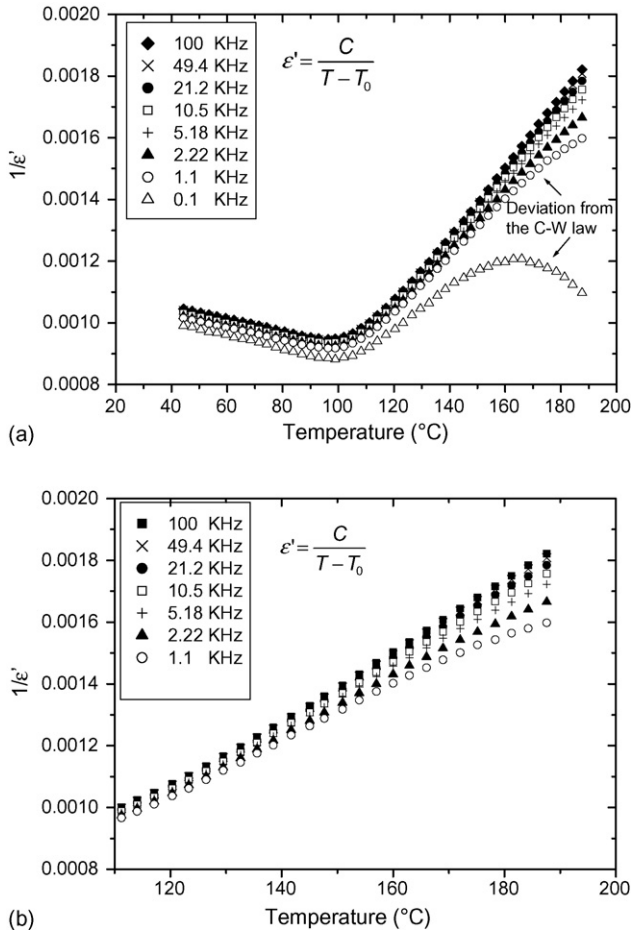

Fig. 14. Reciprocal dielectric constant as a function of temperature at frequencies in the range 0.1–100 kHz: general view (a) and detailed view of the C–W plot (b).

ceramics with grain size in the micron range.[9,13] The progressive depression of the permittivity in $BaTiO_3$ ceramics when the grain size is decreased below 1 μm has been attributed to the existence of a non-ferroelectric grain boundary layer (dead layer) with a thickness independent of the grain size.[42] The grain boundary dead layer exerts a dilution effect on the permittivity of the ceramic because its dielectric constant is much lower (of the order of 100) than that of the ferroelectric region. According to the effective medium approach,[43] the existence of a dead layer with a thickness of 1–2 nm is enough to explain the observed drop of permittivity in nanocrystalline ceramics.[43,13] A strong indication of the existence of a dead layer at the grain boundaries is provided by the significant lowering of the Curie–Weiss temperature observed in the present sample and predicted by the model.[43] Fit of Eq. (3) to the permittivity data for frequencies above 5 kHz gives $T_0 = 19$–$28\,^{\circ}C$ (Table 2), to be compared with a reference value of 110 °C reported for single crystals and coarse ceramics.[8] For ceramics with grain size below 50–100 nm, a decrease of the Curie constant is also expected.[43] Accordingly, the measured Curie constant is $\approx 9 \times 10^4\ K^{-1}$ (Table 2), in comparison with a reference value of $1.8 \times 10^5\ K^{-1}$.

Table 2
Curie–Weiss temperature and Curie constant measured at 1–100 kHz

Frequency (kHz)	Curie–Weiss temperature (°C)	Curie constant (K^{-1})
100	28	8.9×10^4
50	25	8.9×10^4
20	23	9.2×10^4
10	22	9.5×10^4
5	19	9.8×10^4
2	13	10.3×10^4
1	9	10.8×10^4

4. Conclusions

A novel integrated route to produce dense nanostructured $BaTiO_3$ is proposed in this work. Specifically, the method involves the synthesis of a single phase perovskite material by SHS starting from barium peroxide, titanium and titanium oxide. Nanostructured powders are then obtained by ball milling the resulting SHS product under appropriate conditions. It is found that the increase of milling time to 15 h corresponded to the refinement of $BaTiO_3$ crystallite size up to about 15 nm. Moreover, the most significant grain size refinement occurred at the early stages of milling and, after 5 h milling, nanostructured powders with grain sizes in the range 20–30 nm are obtained. When the latter are subjected to the consolidation/sintering step through SPS (700 A, 40 MPa), by properly varying sintering time in the interval 70–140 s, it is possible to obtain products with relative density in the range 66–99%, respectively. This aspect is of practical importance, since the material under investigation find applications either as fully dense product, for instance as capacitor,[5] or when fabricated in porous form, for example as gas sensor devices.

Regarding grain growth during the consolidation stage performed by SPS, it is seen that when electric current is applied for period of time equal or less than 100 s, $BaTiO_3$ grain sizes are maintained below 50 nm, so they are affected only modestly by SPS treatment.

The observed dielectric properties are typical of a nanocrystalline $BaTiO_3$ ceramic. The Curie temperature is shifted to lower temperatures (108 °C) and the relative dielectric constant is significantly depressed by the dilution effect due to the presence of a non-ferroelectric low permittivity grain boundary layer. These observations confirm the existence of remarkable size and grain boundary effects in fine grained barium titanate ceramics.

Acknowledgement

The financial support of MIUR PNR 2001-2003 (FIRB art. 8) D.M. 199 Ric., 8 March 2001 is gratefully acknowledged.

References

1. Sheppard, L., Progress continues in capacitor technology. *Am. Ceram. Soc. Bull.*, 1993, **72**(3), 44–57.

2. Geiger, G., Advances in dielectric ceramics. *Am. Ceram. Soc. Bull.*, 1994, **73**(8), 57–61.
3. Sakabe, Y., Multilayer ceramic capacitors. *Curr. Opin. Solid State Mater. Sci.*, 1997, **2**(5), 584–587.
4. Kotecki, D. E., A review of high dielectric materials for dram capacitors. *Integr. Ferroelectr.*, 1997, **16**(1–4), 1–19.
5. Yoon, D. H. and Lee, B. I., $BaTiO_3$ properties and powder characteristic for ceramic capacitors. *J. Ceram. Process. Res.*, 2002, **3**(2), 41–47.
6. Feteira, A., Sinclair, D. C., Reaney, I. M., Somiya, Y. and Lanagan, M. T., $BaTiO_3$-based ceramics for tunable microwave applications. *J. Am. Ceram. Soc.*, 2004, **87**(6), 1082–1087.
7. Pithan, C., Hennings, D. and Waser, R., Progress in the synthesis of nanocrystalline $BaTiO_3$ powders for MLCC. *Int. J. Appl. Ceram. Technol.*, 2005, **2**(1), 1–14.
8. Lines, M. and Glass, A. M., *Principles and Applications of Ferroelectrics and Related Materials*. Oxford University Press, Oxford, 1977.
9. Arlt, G., Hennings, D. and De With, G., Dielectric properties of fine-grained barium titanate ceramics. *J. Appl. Phys.*, 1985, **58**, 1619–1625.
10. Buscaglia, M. T., Buscaglia, V., Viviani, M., Petzelt, J., Savinov, M., Mitoseriu, L. *et al.*, Ferroelectric properties of dense nanocrystalline $BaTiO_3$ ceramics. *Nanotechnology*, 2004, **15**, 1113–1117.
11. Li, B., Wang, X., Li, L., Zhou, H., Liu, X., Han, X. *et al.*, Dielectric properties of fine-grained $BaTiO_3$ prepared by spark-plasma-sintering. *Mater. Chem. Phys.*, 2004, **83**, 23–28.
12. Luan, W., Gao, L., Kawaoka, H., Sekino, T. and Niihara, K., Fabrication and characterization of fine-grained $BaTiO_3$ ceramics by spark plasma sintering. *Ceram. Int.*, 2004, **30**, 405–410.
13. Zhao, Z., Buscaglia, V., Viviani, M., Buscaglia, M. T., Mitoseriu, L., Testino, A. *et al.*, Grain-size effects on the ferroelectric properties of dense nanocrystalline $BaTiO_3$ ceramics. *Phys. Rev. B*, 2004, **70**, art. no. 024107.
14. Deng, X., Wang, X., Wen, H., Kang, A., Gui, Z. and Li, L., Phase transitions in nanocrystalline barium titanate ceramics prepared by spark plasma sintering. *J. Am. Ceram. Soc.*, 2006, **89**(3), 1059–1064.
15. Anuradha, T. V., Ranganathan, S., Tanu, M. and Patil, K. C., Combustion synthesis of nanostructured barium titanate. *Scripta Mater.*, 2001, **44**, 2237–2241.
16. Kong, L. B., Ma, J., Huang, H., Zhang, R. F. and Que, W. X., Barium titanate derived from mechanochemically activated powders. *J. Alloys Compd.*, 2002, **337**, 226–230.
17. Hakuta, Y., Ura, H., Hayashy, H. and Arai, K., Continuous production of $BaTiO_3$ nanoparticles by hydrothermal synthesis. *Ind. Eng. Chem. Res.*, 2005, **44**, 840–846.
18. Munir, Z. A. and Anselmi-Tamburini, U., Self-propagating exothermic reactions: the synthesis of high-temperature materials by combustion. *Mater. Sci. Rep.*, 1989, **3**, 277.
19. Varma, A., Rogachev, A. S., Mukasyan, A. S. and Hwang, S., Combustion synthesis of advanced materials: principles and applications. *Adv. Chem. Eng.*, 1998, **24**, 79–225.
20. Komarov, A. V. and Parkin, I. P., New routes in the self propagating high-temperature synthesis of barium titanium oxide. *Polyhedron*, 1996, **15**(8), 1349–1353.
21. Suryanarayana, C., Mechanical alloying and milling. *Prog. Mater. Sci.*, 2001, **46**, 1.
22. Takeuchi, T., Tabuchi, M. and Kageyama, H., Preparation of dense $BaTiO_3$ ceramics with submicrometer grains by spark plasma sintering. *J. Am. Ceram. Soc.*, 1999, **82**(4), 939–943.
23. Takeuchi, T., Capiglia, C., Balakrishnan, N., Takeda, Y. and Kageyama, H., Preparation of fine grained $BaTiO_3$ ceramics by spark plasma sintering. *J. Mater. Res.*, 2002, **17**(3), 575–581.
24. Li, B., Wang, X., Cai, M., Hao, L. and Li, L., Densification of uniformly small-grained $BaTiO_3$ using spark-plasma-sintering. *Mater. Chem. Phys.*, 2003, **82**, 173–180.
25. Mustofa, S., Araki, T., Furusawa, T., Nishida, M. and Hino, T., The PLD of $BaTiO_3$ target produced by SPS and its electrical properties for MLCC application. *Mater. Sci. Eng. B*, 2003, **103**, 128–134.
26. Omori, M., Sintering, consolidation, reaction and crystal growth by spark plasma sintering (SPS). *Mater. Sci. Eng. A*, 2000, **287**, 183–188.
27. Nygren, M. and Shen, Z., On the preparation of bio-, nano- and structural ceramics and composites by spark plasma sintering. *Solid State Sci.*, 2003, **5**, 125–131.
28. Hungría, T., Algueró, M., Hungría, A. B. and Castro, A., Dense fine-grained $Ba_{1-x}Sr_xTiO_3$ ceramic prepared by the combination of mechanosynthesized nanopowders and spark plasma sintering. *Chem. Mater.*, 2005, **17**, 6205–6212.
29. Locci, A. M., Orrù, R. and Cao, G., Simultaneous spark plasma synthesis and consolidation of WC/Co composites. *J. Mater. Res.*, 2005, **20**(3), 734–741.
30. Locci, A. M., Orrù, R., Cao, G. and Munir, Z. A., Simultaneous spark plasma synthesis and densification of $TiC–TiB_2$ composites. *J. Am. Ceram. Soc.*, 2006, **89**(3), 848–855.
31. Locci, A. M., Licheri, R., Orrù, R., Cincotti, A. and Cao, G., Synthesis/sintering of dense carbides-, borides- and perovskites- based materials by SPS. *Ceram. Transactions*, 2006, **194**, 173–188.
32. Kawahara, M., Kim, H.-T. and Tokita, M., Fabrication of nano-materials by spark plasma sintering (SPS) method. Proceedings of the Metallurgy World Congress. *Jpn. Soc. Powder Powder Metal.*, 2000, 741–744.
33. Orrù, R., Woolman, J., Cao, G. and Munir, Z. A., The synthesis of dense nanometric $MoSi_2$ through mechanical and field activation. *J. Mater. Res.*, 2001, **16**, 1439–1448.
34. Cincotti, A., Licheri, R., Locci, A. M., Orrù, R. and Cao, G., A review on combustion synthesis of novel materials: recent experimental and modeling results. *J. Chem. Technol. Biotechnol.*, 2003, **78**, 122–127.
35. Halder, N. C. and Wagner, C. N. J., Separation of particle size and lattice strain in integral breadth measurements. *Acta Crystallogr.*, 1966, **20**, 312.
36. JCPDS International Centre for Diffraction Data, 1998.
37. Barin, I., *Thermochemical Data of Pure Substances*. VHC, 1993.
38. Yu, J., Paradis, P. F., Ishikawa, T., Yoda, S., Saita, Y., Itoh, M. *et al.*, Giant dielectric constant of hexagonal $BaTiO_3$ crystal grown by containerless processing. *Chem. Mater.*, 2004, **16**, 3973–3975.
39. Sinclair, D. C., Skakle, J. M. S., Morrison, F. D., Smith, R. I. and Beales, T. P., Structure and electrical properties of oxygen-deficient hexagonal $BaTiO_3$. *J. Mater. Chem.*, 1999, **9**, 1327–1331.
40. Kirby, W. K. and Wechsler, B. A., Phase relations in the barium–titanium oxide system. *J. Am. Ceram. Soc.*, 1991, **74**(8), 1841–1847.
41. Cincotti, A., Murgia, G., Orrù, R. and Cao, G., On the modeling of the copper block combustion front quenching technique to investigate solid–solid self-propagating high-temperature reactions. *Ind. Eng. Chem. Res.*, 2001, **40**, 3451–3458.
42. Frey, M. H., Xu, Z., Han, P. and Payne, D. A., The role of interfaces on an apparent grain size effect on the dielectric properties for ferroelectric barium titanate ceramics. *Ferroelectrics*, 1998, **206–207**, 337–353.
43. Emelyanov, A., Yu Pertsev, N. A., Hoffmann-Eifert, S., Böttger, U. and Waser, R., Grain-boundary effect on the Curie–Weiss law of ferroelectric ceramics and polycrystalline thin films: calculation by the method of effective medium. *J. Electroceram.*, 2002, **9**, 5–16.